Application of ultrasound-tagged photons for measurement of amplitude of vibration of tissue caused by ultrasound: theory, simulation, and experiments

C. Usha Devi
R. M. Vasu
Indian Institute of Science
Department of Instrumentation
Bangalore 560 012, India

A. K. Sood
Indian Institute of Science
Department of Physics
Bangalore 560 012, India

Abstract. We investigate the modulation of an optical field caused by its interaction with an ultrasound beam in a tissue mimicking phantom. This modulation appears as a modulation in the intensity autocorrelation, which is measured by a photon counting correlator. The factors contributing to the modulation are: 1. amplitude of vibration of the particles of the tissue, 2. refractive index modulation, and 3. absorption coefficient in the region of the tissue intercepted by the ultrasound beam and light. We show in this work that a significant part of the contribution to this modulation comes from displacement of the tissue particles, which in turn is governed by the elastic properties of the tissue. We establish, both through simulations and experiments using an optical elastography phantom, the effects of the elasticity and absorption coefficient variations on the modulation of intensity autocorrelation. In the case where there is no absorption coefficient variation, we suggest that the depth of modulation can be calibrated to measure the displacement of tissue particles that, in turn, can be used to measure the tissue elasticity. [DOI: 10.1117/1.2209012]

Keywords: ultrasound-assisted optical tomography; elastography; optical tomography; medical imaging.

Paper 05354R received Nov. 25, 2005; revised manuscript received Jan. 23, 2006; accepted for publication Mar. 3, 2006; published online May 31, 2006.

1 Introduction

Diagnostic imaging with near-infrared (NIR) light is being pursued by many researchers with a view to obtain space-resolved spectroscopic variations in absorption and scattering coefficients of the tissue.[1–3] Since tissue is highly scattering, and light is modeled to diffuse through the tissue, the spatial resolution in the reconstruction is poor with minimum resolvable dimensions of the order of approximately 8 to 10 mm. Selective discrimination of transmitted photons on the basis of whether they have intercepted a region of interest or not is a way to improve resolution by eliminating a multitude of unwanted diffuse photon paths contributing to the transmitted light. This has been achieved by tagging photons with the help of ultrasound insonifying the region of interest.[4–6] The discriminant is the periodic phase correlation picked up by the light through its interaction with the region insonified, which manifests itself as a modulation in the speckle pattern formed by the coherent addition of the ultrasound modulated light with the unmodulated part at the detector outside the tissue. This modulation can be picked up in the intensity autocorrelation measured using a photon counting correlator. The measured modulation depth is used to get a qualitative image of the absorption coefficient at the region of interest. A cross sectional image can be constructed by scanning the probing ultrasound and light beams.

The mechanisms of acousto-optic interaction were modeled in a number of publications in the past.[5,7–12] These studies resulted in the identification of the following mechanisms to model the interaction. In addition to periodic displacement of scatterers, the ultrasound causes periodic compression and decompression of the tissue, resulting in modulation of the refractive index and the absorption coefficient. The periodic displacement and modulation of the refractive index modulate the optical path of light traversed, which gives rise to a phase modulation in the output light. This phase modulation can be observed as an intensity modulation using a coherent detection scheme. This modulation is also related to the local absorption coefficient, which therefore can be used as a read-out for the local absorption coefficient, as is done in ultrasound-assisted optical tomography (UAOT).[13]

The UAOT read-out is accurate only under the assumption that the refractive index modulation and displacement do not vary when we change the insonification region. In tissue, this is known to be true in the case of refractive index, but cannot be assumed for the displacement. The displacement arising out of insonification is also dependent on the local stiffness of the tissue. The modulation of the optical path of photons through displacement variation of scattering particles in the medium subjected to the US force is estimated by Blonigen et

Address all correspondence to R. M. Vasu, Instrumentation, Indian Inst. of Science, C.V. Raman Avenue, Bangalore, Karnataka 560012, India; Tel: 91 80 3942889; Fax: 91 80 3600135; E-mail: vasu@isu.iisc.ernet.in

1083-3668/2006/11(3)/034019/8/$22.00 © 2006 SPIE

al.[14] However, here the displacement suffered by particles owing to pressure from the US is calculated by considering the equation of motion of particles in a viscous medium. The opposing forces on the particles considered are the force from the US beam and the viscous drag, and no elastic property-based restoration force is considered in the model. Indeed, for arriving at displacement suffered by particles in a tissue, local visco-elastic properties are to be considered. However, it is noticed that in many of the publications, the light propagation models in the context of UAOT[7–13] make use of the ultrasound amplitude (and not the displacement suffered by particles on application of the US force) in the expression for phase of detected photons. Since the phase fluctuations owing to displacements are dependent on elastic properties (neglecting viscosity), these fluctuations can be used to map the elastic property of the medium. With this in mind, we revisit UAOT, in which the amplitude or intensity autocorrelation of the transmitted light is measured. Therein we show that the power spectral amplitude at the US frequency obtained from this measurement is influenced by both the local optical property variation (mainly absorption coefficient, because refractive index and its modulation are assumed not to vary in the tissue) and the elastic property variation. Therefore, if the measured modulation is to be used to map either of these properties, the influence of the other has to be properly accounted for. In fact, we show here, both through simulation and experiments, that the influence of the elastic property variation on the depth of modulation in the intensity autocorrelation is greater than that due to the absorption coefficient variation. In the context of eventual application of UAOT for cancer detection on the basis of absorption coefficient (μ_a) increase in malignant tissue, the current UAOT read-out results in erroneous μ_a maps. This is because malignancy manifests itself through a far greater increase ($\sim$2 orders of magnitude) in elastic properties than the optical absorption coefficient.[15,16] If a quantitative map of μ_a is desired through UAOT, which is needed for functional parameters estimation leading to early diagnosis of malignancy,[17–19] compensation for the influence of elastic property is quite necessary. It also becomes evident that an UAOT experiment can also be used to map the elastic property variations in tissue, provided that the effect of absorption coefficient variation is accounted for. Thus, a typical UAOT system can provide an optical probe, with reach deep within the tissue, for displacement measurement. Since displacement can be used to infer elasticity, an UAOT system has potential application for early diagnosis of cancer on the basis of tissue elasticity variation.

A summary of the rest of the work is as follows. In Sec. 2 we describe the Monte Carlo (MC) simulation used to propagate photons through a tissue equivalent phantom to calculate the field autocorrelation at the detectors kept at the boundary of the object. We insonify the object using a parallel sheet of US beam in a direction perpendicular to the probing light beam. We calculate the force applied in the phantom at the region of interaction between the US and light beams through first calculating the US intensity. The force is converted into a displacement field by solving the forward problem of elastography with knowledge of local elastic properties. This displacement field is also made use of in the MC simulation to arrive at the electric field autocorrelation at the boundary. It is seen that the autocorrelation has a sinusoidal modulation whose depth is influenced by both the elastic and optical property variations in the region of the tissue interrogated. In Sec. 3 we describe the experiments carried out to verify these simulation results. In the experiments we make use of an elastography phantom, whose elastic and optical properties can be tailored to known preset values. The light detector system, which has a photon-counting correlator, produces intensity autocorrelations, whose depths of modulation showed variations consistent to what are observed in the simulations. Plots showing power spectral intensity variations in the autocorrelation at the US frequency with optical and elastic properties are also presented, which prove that experimental results closely follow those from the simulations. Discussion of the results are in Sec. 4, and concluding remarks are in Sec. 5.

2 Simulation of Light Propagation Through an Object Insonified by an Ultrasound Beam

We employ MC simulation to model the propagation of photons through a tissue-mimicking phantom insonified by a parallel US beam. The parameters needed for MC simulation are the optical properties of the medium such as absorption coefficient $[\mu_a(r)]$, scattering coefficient $[\mu_s(r)]$, scattering anisotropy factor (g), refractive index $[n(r)]$, and the results of application of the force through the US beam at the location where the photons cross the US beam, such as displacement and modulation in $n(r)$ and $\mu_a(r)$. Of the effects of application of the US beam we neglect two, considering them to be too small for inclusion in the modeling: 1. modulation in absorption, and 2. the change in $\Delta n(r)$, the modulation in refractive index, consequent to changes in local elastic properties. Since our aim is to compute the field correlation of light arriving at the detectors, we keep track of the optical path traversed by the photons in addition to their weights, so that the amplitude of light at the detector can be computed. We first describe how the force exerted by the US beam is used to compute the distribution of displacements in the object. Our region of interest is the volume where the US and light beams intersect.

2.1 *Calculation of the Force Applied by the Ultrasound Beam Inside the Tissue*

The US transducer outputs a plane wave that is coupled into the tissue-mimicking phantom. The transducer has a coupling coefficient k_{eff}^2, so that if $\langle E' \rangle$ is the average energy input to it, only $\langle E \rangle = \langle E' \rangle k_{eff}^2$ is delivered to the phantom at the interface. The average intensity I_0 of the ultrasound beam is related to the average energy as[20]

$$I_0 = \frac{1}{s}\frac{d\langle E \rangle}{dt}, \tag{1}$$

where s the cross sectional area of the US beam, which is taken to be 154 mm^2 to match the transducer used in the experiments. The acoustic and mechanical properties of the phantom are those of the poly-vinyl alcohol (PVA) phantom used in the experiments. They are: 1. average density $\rho = 1012\ kgm^{-3}$, 2. sound velocity $c = 1543\ msec^{-1}$, and 3. acoustic absorption coefficient $\alpha = 1.9\ dBcm^{-1}$ at 1 MHz. The phantom considered is a slab of dimensions $30 \times 10 \times 30$ mm. The depth at which a parallel beam of light is

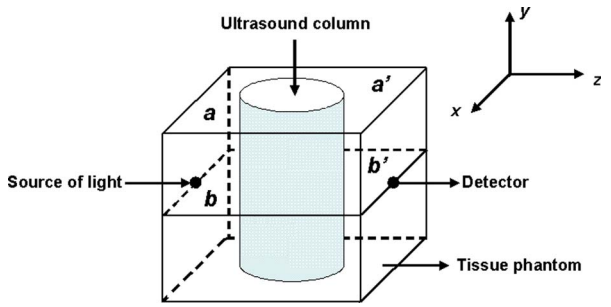

Fig. 1 Description of the object used in the simulations and experiment. The phantom size is 30 ×10 ×30 mm. A plane US transducer is mounted on the top surface of the object, marked as *aa′*, which sends an US beam along the *y* direction. The column of US beam is shown as a cylinder. The object is illuminated with a parallel light beam perpendicular to the US direction in the *x-z* plane marked as *bb′*. The source and detector positions are in the same plane *bb′*.

allowed to intercept perpendicular to the acoustic beam is 5 mm. Since the acoustic absorption coefficient and depth of interrogation are small, the acoustic intensity I at this depth is taken to be approximately equal to the intensity coupled to the phantom from the transducer. The average energy is sinusoidally varying with time and is taken as

$$\langle E\rangle = E\sin(\omega t+\phi), \tag{2}$$

$$\text{and}\quad I=\frac{E\omega}{s}\cos(\omega t+\phi). \tag{3}$$

The radiation force applied to the phantom is given by[21]

$$F=\frac{2\alpha I}{c}=F_0\cos(\omega t+\phi), \tag{4}$$

$$\text{where } F_0=\frac{2E\omega\alpha}{cs}.$$

This radiation force is assumed to be uniform across the cross section of the US beam and is along the propagation direction. The acoustic focusing and diffraction effects are not accounted for in this force calculation.

2.2 *Estimation of the Displacement Field in the Region Interrogated by the Light Beam*

The tissue-mimicking phantom, considered in the previous section and schematically shown in Fig. 1, is a slab with a much smaller thickness in one dimension (y direction) than in the other two. The plane ultrasound transducer mounted on the top surface (aa') sends a column of pressure wave of circular cross section. The object is also illuminated by a plane parallel light beam perpendicular to the US beam. A cross section of the object illuminated, an *x-z* plane for a particular value of y, is denoted as bb' in Fig. 1. We solve a 2-D forward elastography problem to determine the displacement field in the plane bb', which is intercepted and loaded by the force field of the US insonification. Restriction to a 2-D problem is justified only under the assumption that the displacements and their gradients are small throughout the thickness of the object.[22] From the specifications of the transducer used in the experiments, we have calculated that the pressure delivered by the US beam is around 80.6 kPa. Assuming the elastic properties of the fabricated phantom, for the slab under consideration, the displacements are expected to be in the range of 50 to 60 nm. In addition, taking the phantom to be made of a linear elastic material, which is homogeneous, isotropic, and incompressible, the gradients of the displacements in all directions are also expected to be small.

The governing equation for tissue displacement $u=(u_1,u_3)$ loaded by a vibrating force $F\cos\omega t$ along the y axis is given by[23]

$$\mu u_{i,jj}+(\mu+\lambda)u_{j,ji}=\rho\frac{\partial^2 u_i}{\partial t^2}=F\cos\omega t,\quad i=1 \text{ and } 3. \tag{5}$$

Here u_1 and u_3 are the displacements in the directions x and z, ρ is the mass density, λ and μ are the Lame parameters, and subscripts after commas denote partial differentiation with respect to the indices that follow, and summation is implied over repeated indices. The Lame parameters are related to the Young's modulus E^e and Poisson's ratio ν through

$$\lambda=\frac{E^e\nu}{(1+\nu)(1-2\nu)}, \tag{6}$$

$$\text{and}\quad \mu=\frac{E^e}{2(1+\nu)}. \tag{7}$$

The finite element method (FEM) is used to discretize and solve Eq. (5) subject to the Dirichlet boundary condition for displacement on the boundary of the slab (which is far removed from the region of application of the US beam). For the external harmonic loading $F\cos\omega t$, the displacement is also harmonic, denoted by $u\cos(\omega t+\phi)$. The components of u can be solved by inverting the matrix-vector equation resulting from the FEM discretization of Eq. (5). For a set of values of elastic parameters E^e and assuming the Poisson's ratio ν=0.499, Eq. (5) is solved for u_1 and u_3.

2.3 *Modeling of Propagation of Light Through the Insonified Phantom*

In this section, we describe the modeling of interaction of a narrow ultrasound beam with an optical field inside the tissue-mimicking phantom. Analytical models of this interaction of coherent light with US modulated scattering media were developed by many groups in the past. The one we make use of is that developed by Sakadžić and Wang,[11] who considered propagation of light through an US-modulated, anisotropically scattering medium. We also make use of the modification of Monte Carlo (MC) simulation developed by Wang,[10] which has provision to accumulate the optical path taken by individual photons and thus to compute the light field reaching the detector. This enables one to compute the filed autocorrelation of the detected light and, through it, verify the analytical expressions derived for this field autocorrelation.

As pointed out earlier, the propagation of the US wave through a scattering medium causes the medium particles to vibrate, in addition to producing periodic compression and rarefaction to the medium. The vibration amplitude (displace-

ment) of the particle at a point depends on the mechanical properties of the medium in addition to the amplitude of the US beam at that location. The compression and rarefaction produce local density modulations, which for the light beam are refractive index modulations (both real and imaginary parts). Modulation in absorption coefficient (μ_a) resulting from fluctuations in the imaginary part of the refractive index can be picked up by an incoherent light beam as well. As noted in Refs. 10 and 11, this variation in μ_a is too small to result in any detectable intensity fluctuations.

Phase modulation of light caused by displacement as well as the refractive index modulation is picked up only in a coherent addition of light at the detectors, where it appears as an intensity modulation. This intensity modulation is observed as a modulation in the filed autocorrelation function $g_1(\tau)$. In our experiments, we measure the intensity autocorrelation of the detected light $g_2(\tau)$, which is related to $g_1(\tau)$. Publications from Wang and Sakedžić[9–11] have already established procedures for arriving at expressions for $g_1(\tau)$, which have been verified through MC simulations. We make use of these and compute $g_1(\tau)$ [and through it $g_2(\tau)$] both through the analytical expressions and MC simulation. The major modification we have introduced in these procedures, while adapting it to the case of a tissue equivalent phantom with both optical and elastic property variations, is to replace the ultrasound amplitude used in the expression for the phase fluctuations by the displacement distributions caused by the ultrasound-induced force, which is calculated as per the procedure outlined in Sec. 2.2. A minor modification that may become essential when there is a large variation in elastic property is to account for the change in Δn, the refractive index modulation, with elastic properties. In the simulations reported here, we chose to neglect this second-order change in the refractive index. For the sake of completeness, we give a brief summary of these steps used in Ref. 11 to arrive at $g_1(\tau)$.

It is assumed that $g_1(\tau)$ has independent contributions from stochastic fluctuations (S) in phase (contributions from Brownian motion and other temperature-induced movements) and deterministic effects (D) consequent to the application of the US beam. Therefore, the autocorrelation can be expressed as

$$g_1(\tau) = \int_0^\infty p(s)\langle E_s(t)E_s^*(t+\tau)\rangle_S \langle E_s(t)E_s^*(t+\tau)\rangle_D ds. \quad (8)$$

Here, $p(s)$ is the probability density function for s, the path lengths traversed by the detected photons. Contributions to $g_1(\tau)$ from the Brownian motion and the US beam can be considered separately. For the US component, $\langle E_s(t)E_s^*(t+\tau)\rangle_D$ is computed in Ref. 11, under the assumption that the fluctuations introduced are small, as

$$\langle E_s(t)E_s^*(t+\tau)\rangle_D = \exp[-F(\tau)/2], \quad (9)$$

$$\text{where } F(\tau) = \left\{ \left[\sum_{j=1}^{N} \Delta\phi_{n,j}(t,\tau) + \sum_{j=1}^{N-1} \Delta\phi_{d,j}(t,\tau) \right]^2 \right\}, \quad (10)$$

[Eq. (5) of Ref. 11]. Here, $\Delta\phi_{n,j}(t,\tau) = \phi_{n,j}(t+\tau) - \phi_{n,j}(t)$ and $\Delta\phi_{d,j}(t,\tau) = \phi_{d,j}(t+\tau) - \phi_{d,j}(t)$, where $\phi_{n,j}(t,\tau)$ and $\phi_{d,j}(t,\tau)$ are the phase variations arising out of refractive index fluctuations and displacement, along the j'th free path in the photon path connecting source and detector.

Details of computations of $F(\tau)$ are given in Ref. 11. The expressions for $\Delta\phi_{n,j}(t,\tau)$ and $\Delta\phi_{d,j}(t,\tau)$, which have the displacement of particles (u_0: displacement component in the j'th free path) entering in explicitly are given by:

$$\Delta\phi_{nj}(t,\tau) = 4n_0k_0\eta u_0 \sin\left(\frac{\omega_a\tau}{2}\right)\sin\left(\frac{k_a\ell_j\cos\theta_j}{2}\right) \times(\cos\theta_j)^{-1}\cos\left[k_a\hat{e}_a \cdot r_{j-1} + \frac{k_a\ell_j\cos\theta_j}{2} - \omega_a\left(t+\frac{\tau}{2}\right)\right], \quad (11)$$

$$\Delta\phi_{dj}(t,\tau) = 2n_0k_0u_0\sin\left(\frac{\omega_a\tau}{2}\right)\left[(\hat{e}_{j+1} - \hat{e}_j)\cdot\hat{e}_a\right] \times\cos\left[k_a\hat{e}_a \cdot r_j - \omega_a\left(t+\frac{\tau}{2}\right)\right]. \quad (12)$$

Here, ρ is the density of the material of the phantom, $\eta = (\partial n/\partial p)\rho c^2$, with $(\partial n/\partial p)$ being the adiabatic piezo-optic coefficient, θ_j is the angle between the directions of light and US beams, and ω_a is the US frequency. In addition, k_0 and k_a are the moduli of the optical and ultrasound wave vectors, respectively, and ℓ_j is the scattering length in the direction $\hat{e}_j$ at the j'th scattering event. An expression for $F(\tau)$ is arrived at by computing the averages over time and over allowed paths s of the expression on the right-hand side of Eq. (10). An expression for $g_1(\tau)$ is obtained by substituting the expression for $p(s)$ for a semi-infinite slab and the expression for $F(\tau)$ in Eq (8). From $g_1(\tau)$, $g_2(\tau)$ is estimated using the Siegert relation[24] as $g_2(\tau) = 1 + \beta|g_1(\tau)|^2$, where β is a factor determined by the collection optics used for the experiment.

The substantiation of this theoretical result is done by calculating $g_1(\tau)$ through MC simulation. As suggested in Refs. 10 and 11, we have made use of both the reciprocity principle, whereby a point detector is replaced by a large area plane detector, and the similarity relation, which helps speed up the MC simulation by considering l^* the transport mean free-path as the basic step instead of l the scattering mean free path. The perturbation in path length is estimated using the displacement in scattering centers induced by the US force, arrived at by solving the forward elastography equation. We estimate Δn_j using the same displacement and $(\partial n/\partial p)$ value for soft tissue. Contribution to the power spectrum at 1 MHz (the US frequency) is calculated by Fourier transforming $g_2(\tau)$ and estimating the area under the peak at 1 MHz of the spectrum. This power spectral component is proportional to the depth of modulation in $g_2(\tau)$. Variations in the power

spectral amplitude at 1 MHz with respect to local μ_a (with G', the storage modulus, as a parameter) and with respect to G'(with μ_a as a parameter) are plotted. It is seen that results obtained from analytical expressions for $g_2(\tau)$ and the MC simulation matched very well with the experimental data (figures and experiments are described in Sec. 3). More importantly, the modulation in $g_2(\tau)$ is more greatly influenced by G' than by μ_a. The variation in the normalized power spectral amplitude (normalized with respect to the highest value of the set) when the G' varied from 11.4 to 97.3 kPa is from 1 to 0.2408 (μ_a=0.00025 mm^{-1}), whereas μ_a variation from 0.00025 to 0.05 mm^{-1} resulted in variations from 1 to 0.78123 (G'=11.4 kPa). This result is also substantiated through the experiments reported in the next section.

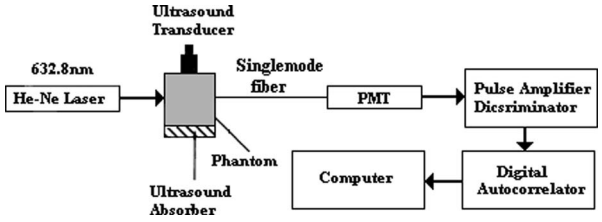

Fig. 2 The experimental setup used to measure the intensity autocorrelation of the transmitted light. The US (1-MHz cw type) and light (He-Ne, 632.8 nm) directions are perpendicular to each other. The photons exiting the object are collected using a single-mode fiber and given to the photon counting PMT. The PMT output is given to the digital autocorrelator.

3 Experiments

3.1 *Phantom Details*

The phantom we have used is made of poly-vinyl alcohol (PVA) gel. The PVA gel is obtained by repeated freezing and thawing cycles of a PVA stock solution of specified hydrolysis.[25–27] By varying the number of freezing-thawing cycles and the residual hydrolysis in the stock solution, we were able to impart porosity (which in turn results in light scattering) and mechanical strength to the resulting gel. The optical absorption is controlled by adding a suitable light-absorbing agent such as India ink of suitable volume and concentration. With this we were able to vary the optical absorption and scattering coefficients from 0.00025 to 0.05 mm^{-1} and 1.441 to 4.5 mm^{-1}, respectively. The range of these values is typical of breast tissues from normal to pathology caused by malignancy.[15,28,29] The physical cross-linking that controls the mechanical strength is also varied, resulting in G' variations from 11.39±0.81 to 149.99±2.12 kPa.These values are also typical of healthy breast tissue and different kinds of malignant tumors found in breast.[16] In addition, the other optical and acoustic properties of the PVA phantom are (with the reported average values for healthy breast tissue shown in brackets[27]): 1. average acoustic velocity 1535.9 m sec^{-1} (1425 to 1575 m sec^{-1}), 2. acoustic impedance 1.5617 $\times 10^6$ kgm^{-2} sec^{-1}(1.425$\times 10^6$ to 1.685$\times 10^6$ kgm^{-2} sec^{-1}), 3. density 1020 kgm^{-3} (1000 to 1007 kgm^{-3}), and 4. refractive index 1.34 at 632.8 nm (1.33 to 1.55 at 589 nm). With this PVA gel, we made a number of slabs of varying mechanical (G' varying from 11.39 to 97.28 kPa) and optical (μ_a varying from 0.00025 to 0.05 mm^{-1} and μ_s' varying from 1.441 to 4.5 mm^{-1}) properties.

3.2 *Intensity Autocorrelation Measurement*

The experimental system to measure the intensity autocorrelation of transmitted photons through the tissue equivalent phantom is shown in Fig. 2. The phantom, which is a slab of dimensions 30$\times$10$\times$30 mm, is insonified using a plane US transducer (continuous-wave type) giving out US radiation at 1 MHz. The coupling medium between the transducer and the phantom is water, into which the phantom is immersed. The insonified phantom (the US beam propagates along the y direction) is illuminated by an unexpanded laser beam from a He-Ne laser (illuminated along the z direction). The exiting photons are collected through a single mode fiber, which ensures a high signal-to-noise ratio by picking up a single speckle for the photon counting system. The photon counting system is a single unit with a PMT and a pulse amplifier discriminator (PAD) (Hamamatsu H7360-03). The output from the photon counting unit is given to an intensity correlator (Flex 021d[30]). The correlator output, which is the intensity autocorrelation $g_2(\tau)$, contains a modulation, the depth of which is dependent on the US-force-induced fluctuations of refractive index and the displacement of particles. The depth of modulation is quantified by measuring the strength of signal at the US modulation frequency in the Fourier transform of the measured autocorrelation. The aim of the experiment is to study the variation in this power spectral amplitude with variations in μ_a and G' of the phantom. As in the case of simulations, it is assumed that variation in fluctuations in the refractive index with a storage modulus is very small and therefore negligible.

The variation in field and intensity autocorrelations with an absorption coefficient is widely reported in the literature.[4,5,9–11] To verify this, we have prepared phantoms with absorption coefficients 0.026, 0.031, and 0.05 mm^{-1} by adding suitable quantities of diluted India ink. The sample phantom prepared without adding any India ink has very little light absorption, for which μ_a is measured to be 0.00025 mm^{-1}. We have also prepared sets of sample phantoms with the prior absorption coefficients with the following storage modulus values: 11.39±0.81, 23.42±0.82, 40.35±1.34, 43.73±0.41, 51.18±0.82, and 97.28±1.23 kPa, following the method described in Sec. 3.1. Using the prior phantoms in the experimental setup of Fig. 2, the intensity autocorrelations are measured. Variations of the power spectral amplitude (obtained from the measured autocorrelations) with absorption coefficient and storage modulus are plotted in Figs. 3 and 4. In each set, the power spectral amplitudes are normalized with respect to the largest value in the set. Each measurement is a result of averaging three separate measurements.

From Figs. 3 and 4, it is clearly seen that the depth of modulation in the autocorrelation is dependent on both μ_a and G' of the medium. In fact, the variation of depth of modulation with G' is much sharper compared to the variations with respect to μ_a. A typical experimentally measured intensity autocorrelation is shown in Fig. 5 (dashed line), which is shown against the theoretical curve obtained for $g_2(\tau)-1$ from MC simulation.

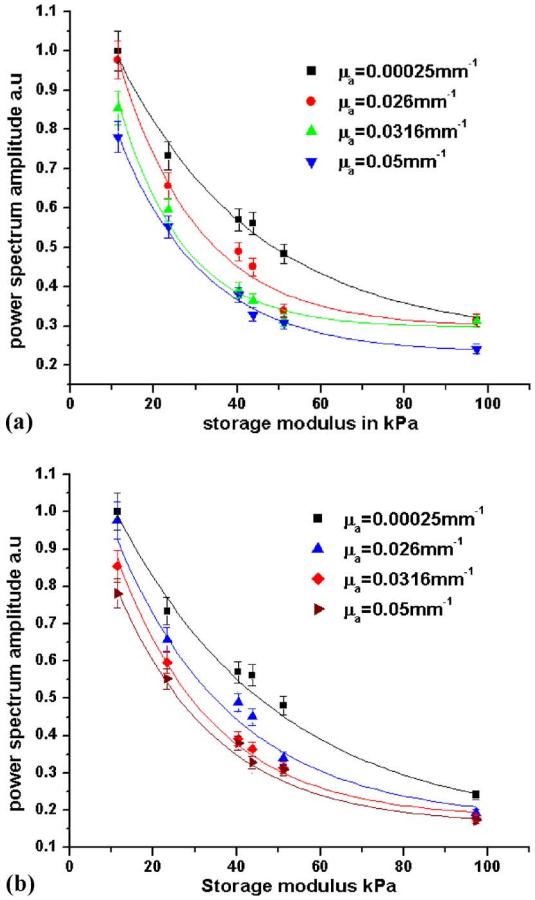

Fig. 3 (a) Variations in the power spectral amplitude at 1 MHz with respect to the storage modulus (G'), with the absorption coefficient as a parameter. The storage modulus is varied from 11.4 to 97.3 kPa, and μ_a values are 0.00025, 0.026, 0.031, and 0.05 mm^{-1}. Solid lines correspond to the results obtained from MC simulations, and symbols with error bars give results obtained from experimental measurements. (b) Same as those given in (a), except that the solid lines here correspond to measurements from analytical expressions for intensity autocorrelations.

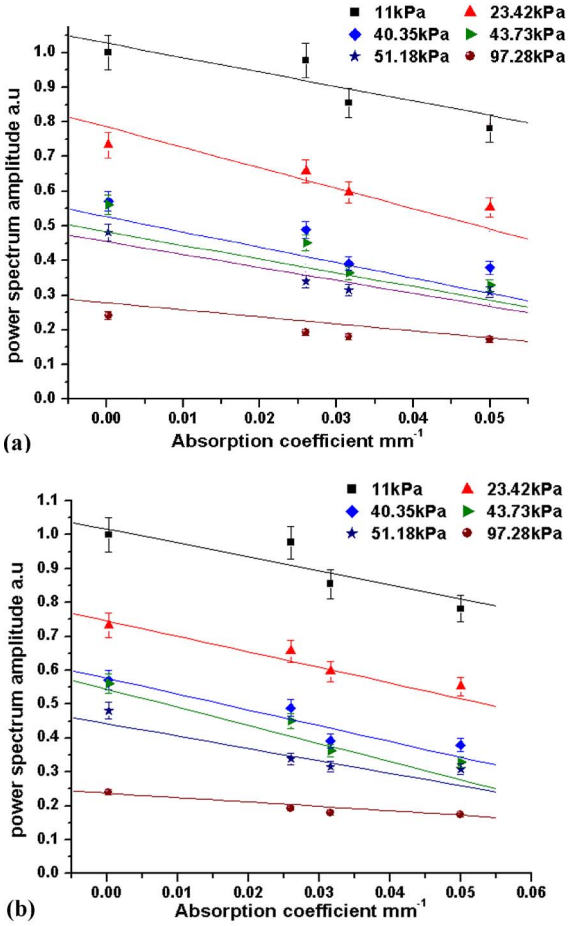

Fig. 4 (a) Variations in the power spectral amplitude at 1 MHz with respect to μ_a (with G' as a parameter). Solid lines correspond to the results obtained from MC simulations, and symbols with error bars give results obtained from experimental measurements. (b) Same as those given in (a), except that the solid lines here correspond to measurements from analytical expressions for intensity autocorrelations.

4 Results and Discussions

It is clearly seen from Figs. 3 and 4 that the variation of the modulation with respect to absorption coefficient and storage modulus, arrived at using the analytical expression given in Ref. 11 and MC simulation, agree with one another. The experimentally measured variations of modulation agree with these theoretical predictions within experimental errors. The variation of the normalized power spectral amplitude is nonlinear with respect to storage modulus and substantial, whereas with respect to μ_a this variation is almost linear. Both the experimental and simulation results show that there is a wide range of variation in the power spectrum amplitude corresponding to a change of approximately one order of magnitude in storage modulus. For example, for μ_a=0.05 mm^{-1}, the power spectral amplitude decreased from around 0.78123 to 0.1734 when G' is increased from 11.4 to 97.3 kPa. But in the case of μ_a variation, corresponding to normal and malignant states of breast tissue, the variation in power spectral amplitude is relatively smaller. Thus, when the storage modulus is 11.4 kPa, the variations in power spectral amplitude (PSA), when μ_a is varied from 0.00025 to 0.05 mm^{-1}, is only from 1.0 to 0.78123. Moreover, when G' is increased, the range of variation in PSA with μ_a has become still smaller. For G' at 51.2 kPa, the range of variation in PSA with μ_a is from 0.4811 to 0.3082. This is to be expected, since with increase in G' the overall modulation depth decreases, and therefore the range of variation on this modulation caused by μ_a (through a multiplication) also decreases. Therefore, the modulation present in the intensity autocorrelation can be used to assess not only the optical property of the location insonified but also its mechanical properties.

5 Conclusion

We show experimentally that the modulation of intensity autocorrelation, caused by insonification of a tissue equivalent phantom by an US beam, is dependant on both the optical and mechanical properties of the phantom. The theoretical prediction of these variations arrived at through both analytical expressions and MC simulations agree well with the corresponding experimental measurements. The modification introduced

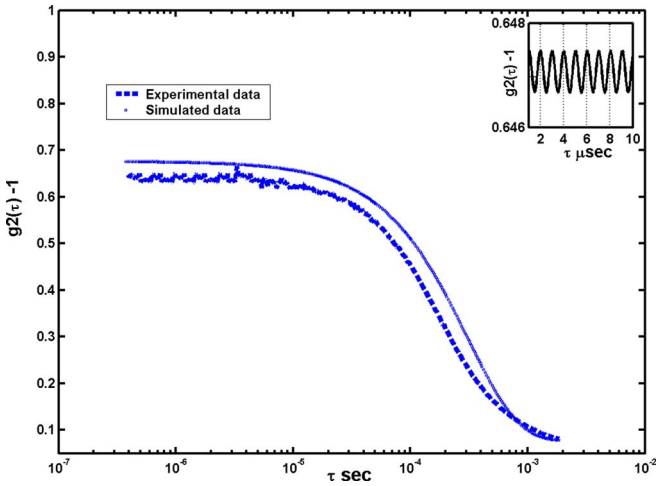

Fig. 5 A typical plot of $g_2(\tau)-1$ with respect to time, obtained experimentally shown against the corresponding result from MC simulation. The dashed line represents the experimental curve and the solid line with * symbol is the simulated data. The inset is a small portion from the experimentally obtained intensity autocorrelation showing the modulation.

in the analytical expressions and simulations compared to earlier published work[8–10] are to substitute ultrasound amplitude with the tissue particle displacement, estimated through solving a forward elastography problem in the region of insonification. It looks feasible to calibrate the modulation depth against tissue displacements, assuming μ_a is constant, and facilitate a read-out of the displacement from the measured autocorrelation modulation. This would pave the way for employing this setup to map the local storage modulus variation through solving an inverse elastography problem, from the measured displacement values.

If the depth of modulation is to be used to arrive at a map of the local absorption coefficients variation, the contribution to the modulation by the elastic property change has to be first ascertained and separated. Since pathological changes due to malignancy are accompanied by both absorption coefficient and elastic property changes, in practical applications of UAOT for tumor detection based on μ_a mapping, compensation for G' variation is mandatory. A separate reconstruction of μ_a distribution is possible from intensity autocorrelation data, which are proportional to the transmitted intensity.[31,32] Once the μ_a distribution is available, the contribution of μ_a to the modulation can be computed and removed from the modulation in the experimentally measured autocorrelation. This compensated data can then be used to reconstruct the storage modulus distribution.

References

1. A. P. Gibson, J. C. Hebden, and S. R. Arridge, "Recent advances in diffuse optical imaging," *Phys. Med. Biol.* **50**, R1–R43 (2005).
2. H. Dehgani, B. W. Pogue, S. P Poplak, and K. D. Paulsen, "Multi-wavelength three-dimensional near-infrared tomography of breast: initial simulation, phantom and clinical results," *Appl. Opt.* **42** 135–145 (2003).
3. A. H. Hielscher, A. Y. Bluestone, G. S. Abdoulaev, A. D. Klose, J. Lasker, M. Stewart, U. Netz, and J. Beuthan, "Near-infrared diffuse optical tomography," *Dis. Markers* **18**, 313–337 (2002).
4. L. V. Wang and X. Zhao, "Ultrasound modulated optical tomography of absorbing objects buried in dense tissue-simulating turbid media," *Appl. Opt.* **36**, 7277–7282 (1997).
5. M. Kempe, M. Larionov, D. Zaslarsky, and A. Z. Genack, "Acousto-optic tomography with multiple scattered light," *J. Opt. Soc. Am. A* **14**, 1151–1158 (1997).
6. S. Leveque, A. C. Boccara, M. Lebec, and H. S. Jalmes, "Ultrasonic tagging of photon paths in scattering media: parallel speckle modulation processing," *Opt. Lett.* **3**, 181–183 (1999).
7. W. Leutz and G. Maret, "Ultrasonic modulation of multiply scattered light," *Physica B* **204**, 14–19 (1995).
8. G. D. Mahan, W. E. Engler, J. J. Tiemann, and E. Uzgiris, "Ultrasonic tagging of light: theory," *Proc. Natl. Acad. Sci. U.S.A.* **95**, 14015–14019 (1998).
9. L. V Wang, "Mechanism of ultrasonic modulation of multiply scattered coherent light: an analytical model," *Phys. Rev. Lett.*, **87**, 043903 (2001).
10. L. V. Wang, "Mechanism of ultrasonic modulation of multiply scattered light: A Monte Carlo model," *Opt. Lett.* **26**, 1191–1193 (2001).
11. S. Sakadžić and L. V. Wang, "Ultrasonic modulation of multiply scattered coherent light: an analytical model for anisotropically scattering media," *Phys. Rev. E* **66**, 026603 (2002).
12. A. Lev and B. Sfez, "*In vivo* demonstration of ultrasound modulated light technique," *J. Opt. Soc. Am. A* **20**, 2347–2354 (2003).
13. G. Yao and L. V. Wang, "Theoretical and experimental studies in ultrasound-modulated optical tomography—biological tissues," *Appl. Opt.* **39**, 659–664 (2000).
14. F. J. Blonigen, A. Nieva, C. A. Dimarzio, S. Manneville, L. Sui, G. Maguluri, T. W. Murray, and R. A. Roy, "Computations of acoustically induced phase shifts of optical paths in acoustophotonic imaging with photorefractive-based detection," *Appl. Opt.* **44**, 3735–3746 (2005).
15. N. Ghosh, S. K. Mohanty, S. K. Majumdar, and P. K. Gupta, "Measurement of optical transport properties of normal and malignant human breast tissue," *Appl. Opt.* **40**, 176–184 (2001).
16. T. A. Krouskop, T. M. Wheeler, F. Kallel, B. S. Garra, T. Hall, and J. Lorenzen, "Elastic moduli of breast and prostrate tissues under compression," *Ultrason. Imaging* **20**, 260–274 (1998).
17. T. O. McBride, B. W. Pogue, E. D. Gerety, S. B. Poplack, U. L. Osterberg, and K. D. Paulsen, "Spectroscopic diffuse optical tomography for the quantitative assessment of hemoglobin concentration and oxygen saturation in breast tissue," *Appl. Opt.* **38**, 5480–90 (1999).
18. B. W. Pogue, S. P. Poplack, T. O. McBride, W. A. Wells, K. S. Osterman, U. L. Osterberg, and K. D. Paulsen, "Quantitative hemoglobin tomography with diffuse near-infrared spectroscopy: Pilot results in the breast," *Radiology* **218**, 261–266 (2001).
19. E. Heffer, V. Pera, O. Schutz, H. Siebold, and S. Fantini, "Near-infrared imaging of the human breast: complementing hemoglobin concentration maps with oxygenation images," *J. Biomed. Opt.* **9**(6), 1143–51 (2004).
20. E. Konofagou, J. Thierman, and K. Hynynen, "A focused ultrasound method for simulation diagnostic and therapeutic applications—a simulation study," *Phys. Med. Biol.* **46**, 2967–2984 (2001).
21. K. R. Nightingale, M. L. Palmeri, R. W. Nightingale, and G. E. Trahey, "On the feasibility of remote palpation using acoustic radiation force," *J. Acoust. Soc. Am.* **110**, 625–634 (2001).
22. O. C. Zienkiewicz and R. L. Taylor, *Finite Element Method*, Vol. **2**, Mc Graw Hill, UK (1991).
23. D. Fu, S. F. Levinson, S. M. Gracewskig, and K. J. Parker, "Noninvasive quantitative reconstruction of tissue elasticity using a iterative forward approach," *Phys. Med. Biol.* **45**, 1495–1509 (2000).
24. S. E. Skipetrov and I. V. Meglinskiĭ, "Diffusing–wave spectroscopy in randomly inhomogeneous media with spatially localized scatterer flows," *J. Exp. Theor. Phys.* **86**, 661–665 (1998).
25. A. Kharine, S. Manohar, R. Seeton, R. G. M. Kolkman, R. A. Bolt, W. Steenbergen, and F. F. M. de Mul, "Poly (vinyl alcohol) gels for use as tissue phantoms in photoacoustic mammography," *Phys. Med. Biol.* **48**, 357–370 (2003).
26. C. M. Hassan and N. A. Peppas, "Structure and applications of poly (vinyl alcohol) hydrogels produced by conventional cross linking or by freezing thawing methods," *Adv. Polym. Sci.* **153**, 37–65, (2000).
27. C. Usha Devi, R. M. Vasu, and A. K. Sood, "Design, fabrication and characterization of tissue—Equivalent phantom for optical elastography," *J. Biomed. Opt.* **10**, 044020 (2005).
28. P. Taroni, A. Torricelli, L. Spinelli, A. Pifferi, F. Apraia, G. Danesini,

and R. Cubeddu, "Time-resolved optical mammography between 637 and 985 nm: clinical study on the detection and identification of breast lesions," *Phys. Med. Biol.* **50**, 2469–2488 (2005).
29. L. Spinelli, A. Torricelli, A. Pifferi, P. Taroni, G. M. Danesini, and R. Cubeddu, "Bulk optical properties and tissue components in the female breast from multi-wavelength time-resolved optical tomography," *J. Biomed. Opt.*, **9**(6), 1137–42 (2004).
30. See http://www.correlator.com, 15 Colmart Way, Bridgewater, NJ 08807.
31. A. H. Hielscher, A. D. Klose, and K. M. Hansen, "Gradient-based iterative image reconstruction scheme for time-resolved optical tomography," *IEEE Trans. Med. Imaging* **18**, 262–271 (1999).
32. A. D. Klose and A. H. Hielscher, "Iterative reconstruction scheme for optical tomography based on the equation of radiative transfer," *Med. Phys.* **26**, 1698–1707 (1999).